Atlas-Based Segmentation of the Subthalamic Nucleus, Red Nucleus, and Substantia Nigra for Deep Brain Stimulation by Incorporating Multiple MRI Contrasts

Yiming Xiao[1], Lara Bailey[1], M. Mallar Chakravarty[2,3], Silvain Beriault[1], Abbas F. Sadikot[4], G. Bruce Pike[1], and D. Louis Collins[1]

[1] Montreal Neurological Institute, McGill University, Montreal, Canada
[2] Kimel Family Translational Imaging Genetics Laboratory, The Centre for Addiction and Mental Health, Toronto, Canada
[3] Department of Psychiatry, University of Toronto, Toronto, Canada
[4] Division of Neurosurgery, McGill University, Montreal, Canada

Abstract. Deep brain stimulation (DBS) of the subthalamic nucleus (STN) is an effective therapy for drug-resistant Parkinson's disease (PD). Pre-operative identification of the STN is an important step for this neurosurgical procedure, but is very challenging because of the accuracy necessary to stimulate only a sub-region of the small STN to achieve the maximum therapeutic benefits without serious side effects. Previously, a technique that automatically identified basal ganglia structures was proposed by registering a 3D histological atlas to a subject's anatomy shown in the T1w MRI image. In this paper, we improve the accuracy of this technique for the segmentation of the STN, substantia nigra (SN), and red nucleus (RN). This is achieved by using additional MRI contrasts (i.e. T2*w and T2w images) that can better visualize these nuclei compared to the sole T1w contrast used previously. Through validation using the silver standard ground truth obtained for 6 subjects (3 healthy and 3 PD), we observe significant improvements for segmenting the STN, SN, and RN with the new technique when compared to the previous method that only uses T1w-T1w inter-subject registration.

1 Introduction

Parkinson's disease (PD) is a progressive and chronic disease of the central nervous system (CNS). Deep brain stimulation (DBS) at the dorsal-lateral site of the subthalamic nucleus (STN) is an effective treatment for relieving motor symptoms (tremor, akinesia, rigidity) of Parkinson's disease [1]. Determining the geometry of the STN is an important step before locating the motor-function region (or dorsal-lateral site) for this neuro-surgical procedure because stimulation of only this sub-region results in desirable therapeutic benefits without side effects. Yet, locating the precise stimulation target is difficult because the STN is small and is in close proximity to several delicate structures, such as the red

P. Abolmaesumi et al. (Eds.): IPCAI 2012, LNAI 7330, pp. 135–145, 2012.

nucleus (RN) and the substantia nigra (SN). Many methods have been proposed previously to locate the stimulation targets [1], and are divided into direct and indirect targeting methods. Direct targeting methods [1] rely on MRI sequences that directly visualize the geometry of the STN. Among these, susceptibility-based methods (i.e. T2*w images and R2* maps) offer better contrast [2] while the T2w Fast-Spin-Echo (FSE) acquisitions are more commonly used [1]. Either way, manual identification is still necessary to determine the target stimulation site. Indirect methods often involve deformation of brain atlases [1]. These procedures need less expert supervision, but the T1w-MRI-based registration may be sub-optimal since the structures of interest are not well visualized in the T1w images, and their locations must be indirectly inferred from nearby structures that have contrast on the T1w image. In this article, we propose a framework that non-rigidly deforms a digitalized histological basal ganglia atlas to segment the STN, RN, and SN by incorporating multiple MRI contrasts to estimate the deformation field. This automatic method was validated with manual segmentations of *in vivo* MRI data acquired on a 3T scanner (Siemens Tim Trio, Erlangen, Germany), and was compared with the T1w-based method introduced previously in [3]. This improved alignment will facilitate more accurate automatic delineation of the sub-region of the STN for the DBS procedure, which requires sub-millimeter accuracy in the stimulation electrode placement.

Fig. 1. A coronal view of the 3D digital basal ganglia atlas (A) and its resulting T1w pseudo-MRI (B) and T2w pseudo-MRI (C)

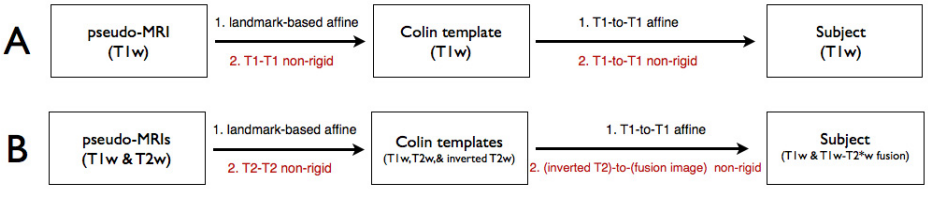

Fig. 2. Pipelines of two atlas-based segmentation schemes. A: atlas-based segmentation method with T1w-T1w registration; B: atlas-based segmentation method with multiple image contrasts incorporated. Differences between A and B are shown in red fonts.

2 Atlas-Warping Segmentation with T1w-T1w Registration

Previously, a high-resolution 3D digital basal ganglia atlas (Fig. 1A) was derived from a post-mortem healthy brain [4]. In addition, a framework to deform this atlas for segmenting basal ganglia structures on an individual's anatomy was also proposed and validated for the globus palllidus (GP), striatum, and thalamus [3]. This segmentation framework only employed T1w images, and the deformation of the basal ganglia atlas was completed in two steps using a global affine and local non-rigid registration strategy. A flow-chart demonstrating the procedure is shown in Fig. 2A. In the first step, the atlas was fitted to the T1-weighted (T1w) Colin27 brain template (Fig. 3A) [5], and this was achieved in two stages. In the first stage, the brain atlas was aligned to the Colin27 template with an affine transformation based on the estimate of 24 homologous landmarks pairs (details in [3]). These homologous landmark pairs were selected on structures well visible on the T1w images, such as the striatum, the lateral ventricle, and thalamus. In the second stage, a pseudo-MRI (Fig.1B) was created by manually assigning each atlas label the intensity value in the corresponding region of the T1w Colin27 template. Then, with ANIMAL non-linear registration [6], this T1-appearing pseudo-MRI was non-rigidly registered to the Colin27 template to further refine the fit between the atlas and the template. After the deformation, the digital brain atlas was brought into the space of Colin27 template. In the second step, the Colin27 template and the co-registered atlas were mapped to the anatomy of a subject seen on the T1w MR image. This was completed in a similar manner as the first step, except the affine transformation was completed automatically using a hierarchical approach with cross-correlation for the cost function. In [3], three variants of the atlas-to-subject registration methods were compared. Based on the segmentation quality of the T1w visible brain structures (i.e. GP, thalamus, and striatum), the strategy described above was considered to be the optimal approach. However, while this atlas-based segmentation technique is robust for

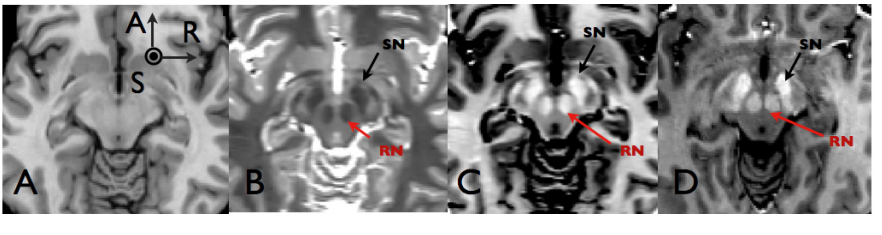

Fig. 3. Images (axial view) used in the proposed automatic nuclei segmentation framework. A=T1w Colin27 template; B=T2w Colin template; C="intensity inverted" T2w Colin template; D=T1w-T2*w fusion image of a healthy female subject. Please note that A-C are in Talairach space, and D is in the native space. The STN and RN are identified in B-D.The coordinates in Talairach space are marked in A, where A=anterior, R=right, and S=superior.

structures easily identifiable on T1w images, its segmentation performance on the STN, RN, and SN may still require further improvement due to the poor contrast of these nuclei in the T1w images, and thus their anatomical variability is not as fully accounted for as other structures (i.e. ventricles, striatum, etc.).

3 Atlas-Warping Segmentation with Multiple MRI Contrasts Registration

At present, FSE T2w MRI images are considered to be the state of the art image acquisition technique to directly visualize the nuclei, such as the STN, SN, and RN. However, the drawback lies in the long scanning times required to achieve high resolution full brain coverage (i.e. $1\times1\times1mm^3$), and it is not perfect for DBS target planning in patients with movement disorders. In addition, the specific absorption rate (SAR) for FSE sequences is often higher than the gradient-echo (GRE) sequences. Recent developments have led to new MRI techniques for visualizing the STN. Among these, the susceptibility-based MRI methods, such as the T2*w image and R2* (1/T2*) map, have demonstrated comparable or better contrast of the STN than the FSE T2w sequences, while providing a higher resolution in a relatively clinically feasible time. We hypothesize that by incorporating the MRI techniques which can directly visualize the STN, SN, and RN into the framework introduced in the previous section, the non-rigid registration should improve the atlas-to-template warping, the template-to-subject warping, as well as the resulting atlas-to-subject warping. As a result, the overall segmentation accuracy should increase. The previous technique in [3] uses T1w-image registration only. While preserving the parameters of the global affine and local non-rigid registration strategy in [3], here we used a T2w-appearing pseudo-MRI, a T2w Colin template, an "intensity-inverted" T2w Colin template, and T1w-T2*w fusion MRI images of the subjects for the local non-rigid registration. Note that the pipeline of this new framework is illustrated in Fig. 2B. The creation the new MRI modalities and the registration procedures are detailed in the following sections.

3.1 T2w Colin MRI Template and T2w Pseudo-MRI

Since the Colin27 T1w template was not able to provide sufficient contrast for the STN and its neighboring SN and RN, a co-aligned T2w FSE Colin template and its corresponding T2w pseudo-MRI were created. First, the T2w Colin template was produced from 12 FSE T2w MR images ($1 \times 1mm^2$ in-plane resolution, $2mm$ slice thickness in sagittal direction) of the same subject as the Colin27 T1w template ([5]). Each T2w image was processed using the following sequence: 1) rigid registration to Colin27 T1w template using normalized mutual information as the objective function [7] and resampling to the Colin27 template grid with sinc-function interpolation; 2) image intensity inhomogeneity correction [8]; 3) image intensity normalization [9]; and 4) non-local means image de-noising [10]. Lastly, the T2w Colin template (Fig. 3B) was generated by averaging these

12 pre-processed images. In this resulting T2w average template, the GP, STN, SN, and RN demonstrate their characteristic hypo-intensity features, while their boundary delineations were improved due to image averaging. The creation of the T2w pseudo-MRI (Fig. 1C) follows the same manner as the original T1w pseudo-MRI except that the intensity values were taken from the Colin T2w image instead of the Colin27 T1w image.

3.2 Inverted T2w Colin Template and T1w-T2*w Fusion Image

Ideally, one would register T2w FSE patient data with the new Colin T2w template to customize the atlas to the patient's anatomy. Unfortunately, it is difficult, if not impossible, to acquire high resolution T2w FSE in clinically acceptable times. We proposed to acquire data with a 10-echo 3D FLASH MRI sequence [11], with the following parameters: echo time (TE)={1.6, 4.1, 6.6, 9.1, 13.0, 16.0, 18.5, 21.0, 23.5, 26.0}ms, repetition time (TR) =30 ms, flip-angle=23^o, read out bandwidth=±450 Hz/pix, acquisition matrix=256x256, 176 sagittal slices, resolution=$0.95\times0.95\times0.95mm^3$, 6/8 partial Fourier in the phase and slice encoding directions, and GRAPPA factor =2, acquisition time = 7:05 min. From the MRI data acquired, three original image contrasts (T1w image, T2*w image, and R2* map) were generated. The T1w image was produced by averaging the magnitude images of the first four echoes. The T2*w image was generated by averaging the magnitude images of the last five echoes. The R2* map was derived by least-square fitting all magnitude data to an exponential curve. These three image contrasts are shown in Fig. 4 for a healthy female subject. Since all three image contrasts were generated in the same scan session, no inter-contrast registration is necessary. The T2*w image and R2* map were used later to establish the silver standard ground truth for evaluation. While non-linear registration of the Colin FSE T2w image and the T2*w patient image might be possible with a mutual information based cost function, we propose to use ANIMAL cross-correlation-based non-linear registration of an "intensity-inverted" T2w Colin template (Fig. 3C) and a T1w-T2*w fusion patient image (Fig. 3D). The patient's fusion image is synthesized using $I_{fusion} = I_{T1w} + (I_{T1w} - I_{T2*w} \times \alpha)$, where I_{fusion}, I_{T1w}, and I_{T2*w} represent the voxel intensities of the fusion image, T1w image, and T2*w image, respectively, and α is the normalization factor that ensures the voxel intensity of the white matter in the T2*w image is at the same level as the T1w image. Last, the "intensity-inverted" T2w Colin template is simply obtained by subtracting the intensity of the T2w Colin template from its maximum value. The use of cross-correlation objective function is justified by the similar image contrast of the two synthesized images (Fig. 3C and 3D), and enables direct comparison with the previous T1w-T1w technique [3].

3.3 Atlas-to-Subject Registration

As shown in Fig. 2B, the new multi-contrast atlas-based customization procedure was completed in two steps. In the first step, the atlas was fitted to the Colin templates. This was done in two stages: First, the previously computed

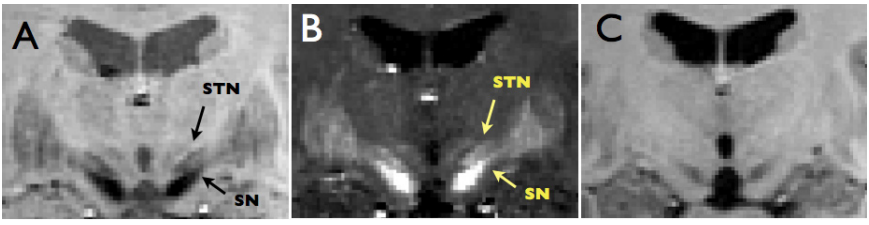

Fig. 4. Coronal slices of T2*w image (A), R2* map (B), and T1w image (C) obtained from the 10 echo 3D FLASH sequences for a healthy female subject. The STN and SN are identified in A and B, but are poorly visualized in C.

landmark-based affine registration [3] brought the atlas roughly to the space of Colin27; Second, local non-rigid registration (in the region of the basal ganglia) was used to fine-tune the remaining anatomical differences between the atlas and Colin27. This step was performed by deforming the T2w basal ganglia pseudo-MRI to the T2w Colin MRI template. In the second half of the pipeline, the Colin template anatomy was brought into each individual's anatomy in two stages. First, an affine registration between the T1w Colin27 template and a subject's T1w image was performed. Susceptibility artifacts (signal drop-outs near the sinus, orbitofrontal and temporal lobes) exist for T2*w MRI, but not for T2w or T1w MRI. Thus, the fusion image has unwanted artifacts near the cortical surface, and for the global affine registration, we think T1-T1 registration is a sufficient and better choice. The "intensity-inverted" T2w Colin template, co-registered with the Colin27 template, was then warped to the T1w-T2*w fusion image of the subject through a local non-rigid registration procedure. Finally, the digital brain atlas was warped using the recovered transformations to the designated subject's anatomy in order to segment the basal ganglia. In the entire pipeline, the registration parameters remained the same as the original T1w-image only framework [3]. Although it is possible to achieve the non-rigid registration by considering a pair of MRIs (T1w and an additional contrast) simultaneously, we feel that using the T2w and fusion images alone is sufficient since the structural information in T1w images is still included in these images for the region of interest, and pair-wise multi-contrast registration is computationally more expensive.

4 Evaluation

4.1 Subjects and Establishment of Ground Truth

After providing informed consent, 3 healthy subjects (1 female, 2 male, age= 37±12yr) and 3 PD patients (1 female, 2 male, age=54±4 yr) volunteered for the study. Each subject was scanned with the proposed 10-echo 3D FLASH MRI sequence. From the acquired MRI data, the T1w image, T2*w image, R2* map, and T1w-T2*w fusion image were produced for each subject. Two sets

of silver standard ground truth for the STN, SN, and RN were made by one expert's manual identification on the MRI images: 1. ground truth for Colin (called "**GT1**"); 2. ground truth for each testing subject (called "**GT2**"). The first set was used to examine the quality of atlas-to-template registration, and the second set was applied to validate the quality of the template-to-subject registration, as well as the segmentation performance of the entire system for the STN, RN, and SN. With ITK-SNAP (www.itkSNAP.org), we obtained the ground truth for the Colin template by manually painting the labels of the STN, SN, and RN on the T2w Colin template in 3D. For all 6 subjects, the manual labels were painted using a consensus of the patient's T2*w image and R2* map.

4.2 Evaluation Methods

In total, three aspects of the final atlas-warping pipeline were examined with respect to segmenting the STN, SN, and RN: 1. quality of atlas-to-template registration; 2. quality of template-to-subject registration; 3. the segmentation performance of the entire system for the nuclei of interest. For the atlas-to-template registration, we compared the Colin27-coregistered histological atlas with the manual segmentation of T2w Colin template ("**GT1**"); In the second aspect, "**GT1**" was employed as an atlas label set and warped to a subject's anatomy with the deformation matrix obtained in the second half of the pipeline, then compared to "**GT2**" in the native space of each subject. Last, the deformed histological atlas was compared with the manually painted labels of each subject ("**GT2**"). For each test, three evaluation metrics were computed to compared the warped labels and the ground truth: 1) the overlap metric **kappa=2*a/(b+c)**, where **a** is the intersection of two segmentations, and **b** and **c** are volumes of each segmentation; 2) the Euclidean distance (COM_{Euclid}) between the centre of mass (COM) of the deformed labels and the silver standard ground truth; and 3) the COM coordinate differences ($\Delta COM_{R,A,S} = COM_{atlas}\text{-}COM_{ground-truth}$) after transforming them into the Talairach space (the coordinates are shown in Fig. 3A). The evaluation results were analyzed using one-sample or paired-sample one-sided t-tests. In the next section, we compared all these metrics for both the original T1w-image-only pipeline, and the newly proposed pipeline with multiple image contrasts added.

4.3 Results

A qualitative examination was conducted between the warped-atlases and the manually identified ground truth for both Colin and the 6 testing subjects. Figure 5 shows coronal views of the warped labels and the manual segmentation of the SN, STN, and RN, overlaid on Colin's and a healthy subject's T1w images. In Fig. 5, the first row (Fig. 5B, 5D, and 5F) shows the result of the registration method in [3]; the second row (Fig. 5C, 5E, and 5G) demonstrates the results of our updated registration framework. From the visual inspection, we are able to see the warped labels in the second row demonstrate higher resemblance with the ground truths for both Colin (**GT1**) and the subject (**GT2**).

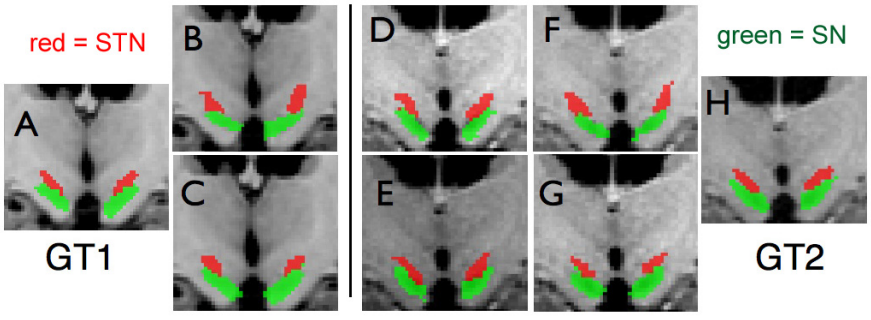

Fig. 5. Results of atlas registration and the silver standard ground truth. A=**GT1**, H=**GT2**. B, D and F are segmentation results of atlas-to-template registration, template-to-subject registration, and complete system, respectively, by using only T1w-T1w registration. C, E and G are segmentation results of atlas-to-template registration, template-to-subject registration, and complete system, respectively, by using multiple image contrasts. Please note that to the **left** of the black line, Image A, B, and C show the labels of Colin; to the **right** side, labels are shown for a healthy female subject.

The quantitative differences between the method in [3] and our updated technique for atlas-to-template registration, template-to-subject registration, and segmentation performance of the complete system, are listed in Table 1, 2, and 3, respectively.

Comparing the results obtained by the two procedures, in general, our new method improves the two registration stages (atlas-to-template and template-to-subject), as well as the segmentation performance of the overall system. For the atlas-to-template registration, improvements are seen for the three metrics for RN and STN. For the SN, while the kappa value increased, the distance

Table 1. Evaluation of atlas-to-template registration. The results of T1w registration are shown in **bold black**, and results of our multi-contrast method are shown in blue. For $\Delta COM_{R,A,S}$, R, A, and S represent the right, anterior, and superior-directions respectively in Talairach space. The same formatting applies to Table 2 and 3.

Side	Metric	RN			SN			STN		
Left	**kappa**	**0.39**			**0.45**			**0.52**		
		0.83			0.56			0.71		
	COM_{Euclid}**(mm)**	**3.14**			**3.51**			**2.41**		
		0.40			3.87			0.35		
	$\Delta COM_{R,A,S}$**(mm)**	R	A	S	R	A	S	R	A	S
		-0.85	**2.30**	**1.97**	**1.45**	**-3.20**	**0.09**	**-1.74**	**0.70**	**1.51**
		-0.38	0.12	0.07	1.53	-3.09	-1.74	0.00	-0.12	0.33
Right	**kappa**	**0.43**			**0.50**			**0.42**		
		0.79			0.60			0.67		
	COM_{Euclid}**(mm)**	**3.09**			**3.36**			**3.15**		
		0.38			3.60			0.57		
	$\Delta COM_{R,A,S}$**(mm)**	R	A	S	R	A	S	R	A	S
		1.70	**1.17**	**2.30**	**-1.07**	**-3.18**	**0.12**	**1.75**	**0.10**	**2.62**
		0.32	0.19	0.03	-1.35	-2.74	-1.92	-0.01	0.19	0.54

Table 2. Evaluation of template-to-subject registration

Side	Metric	RN			SN			STN		
Left	**kappa**	**0.72±0.05** 0.77±0.03			**0.56±0.06** 0.64±0.03			**0.55±0.08** 0.62±0.04		
	COM_{Euclid}**(mm)**	**1.12±0.39** 0.66±0.13			**2.42±0.56** 1.90±0.63			**1.42±0.63** 1.30±0.13		
		R	A	S	R	A	S	R	A	S
	$\Delta COM_{R,A,S}$**(mm)**	**0.31 ±0.51** 0.37 ±0.18	**-0.87 ±0.50** -0.35 ±0.23	**-0.50 ±0.19** -0.31 ±0.29	**0.38 ±0.55** 0.05 ±0.47	**1.95 ±1.34** 1.57 ±1.18	**-0.79 ±0.42** -0.19 ±0.42	**0.26 ±0.64** 0.35 ±0.58	**-0.86 ±1.04** -0.52 ±0.72	**-0.50 ±0.65** -0.85 ±0.21
Right	**kappa**	**0.72±0.07** 0.77±0.04			**0.58±0.10** 0.68±0.05			**0.52±0.08** 0.62±0.06		
	COM_{Euclid}**(mm)**	**0.92±0.39** 0.40±0.18			**1.99±0.77** 1.74±1.03			**1.52±0.63** 1.04±0.63		
		R	A	S	R	A	S	R	A	S
	$\Delta COM_{R,A,S}$**(mm)**	**-0.19 ±0.74** -0.36 ±0.17	**-0.48 ±0.27** -0.10 ±0.20	**-0.49 ±0.26** 0.05 ±0.10	**0.16 ±0.33** 0.12 ±0.33	**1.62 ±1.30** 1.59 ±1.38	**-0.75 ±0.23** -0.02 ±0.26	**0.32 ±1.05** 0.17 ±0.72	**-0.34 ±0.98** -0.14 ±0.68	**-0.69 ±0.48** -0.41 ±0.61

Table 3. Evaluation of the segmentation performance of the overall system

Side	Metric	RN			SN			STN		
Left	**kappa**	**0.54±0.06** 0.82±0.01			**0.55±0.08** 0.59±0.07			**0.56±0.08** 0.63±0.06		
	COM_{Euclid}**(mm)**	**1.85±0.22** 0.43±0.12			**2.54±1.33** 3.39±1.23			**1.58±0.64** 1.08±0.18		
		R	A	S	R	A	S	R	A	S
	$\Delta COM_{R,A,S}$**(mm)**	**-0.23 ±0.55** -0.02 ±0.20	**1.58 ±0.15** -0.30 ±0.18	**1.00 ±0.18** -0.18 ±0.21	**1.71 ±0.64** 2.02 ±0.42	**-1.95 ±1.16** -2.02 ±1.07	**-0.53 ±0.45** -2.04 ±0.59	**-1.22 ±0.51** 0.38 ±0.58	**-0.19 ±0.98** -0.49 ±0.55	**0.60 ±0.53** -0.52 ±0.37
Right	**kappa**	**0.52±0.13** 0.84±0.03			**0.59±0.04** 0.57±0.06			**0.43±0.16** 0.61±0.06		
	COM_{Euclid}**(mm)**	**2.28±0.62** 0.26±0.09			**1.90±1.14** 3.01±0.68			**2.52±0.80** 0.94±0.44		
		R	A	S	R	A	S	R	A	S
	$\Delta COM_{R,A,S}$**(mm)**	**1.56 ±0.80** -0.01 ±0.18	**0.95 ±0.20** 0.09 ±0.15	**1.53 ±0.30** -0.07 ±0.14	**-0.81 ±0.48** -1.38 ±0.42	**-1.55 ±1.12** -1.63 ±1.03	**-0.32 ±0.37** -2.09 ±0.32	**1.84 ±1.13** 0.32 ±0.69	**0.43 ±0.87** -0.08 ±0.69	**1.52 ±0.34** -0.09 ±0.52

measures didn't demonstrate improvements. For the template-to-subject registration, the improvement is significant ($p<0.05$) for the kappa metrics (SN, left RN, and right STN) and COM_{Euclid} (RN and left SN). For the segmentation of the complete system, the enhancement in segmentation performance is significant for the kappa metrics (STN, RN, and left SN), and COM_{Euclid} (RN and right STN). The COM_{Euclid} of the STN (Left:1.08±0.18 mm, Right:0.94±0.44 mm) is in the same range or better than those previously reported [1]. From the analysis of $\Delta COM_{R,A,S}$, we observed a systematic location bias in the warped atlas when using only T1w-T1w inter-subject non-rigid registration: for the template-to-subject registration, the warped labels are more posterior and inferior for the RN ($p<0.05$), and more anterior and inferior for the SN ($p<0.05$). For the complete system, the segmentations are more lateral and superior for the STN, more medial and posterior for the SN ($p<0.05$), and more anterior and superior for the RN ($p<0.05$). However, with our method, the final segmentation

results of the entire system show almost no significant displacement for the RN; although the segmented left STN is more inferior ($p<0.05$), the absolute mean displacement is less than using the old method.

5 Discussion

For the SN segmentation after adding multiple MRI contrasts, the average Euclidean distance between the COMs increased while the kappa metrics improved. Since the mean Hausdorff distance of the SN between the manual and automatic segmentation is smaller with our method (Left: 6.11mm; Right: 5.63mm) than with the T1w registration (Left: 6.72mm; Right: 6.19mm), this can be explained by a tighter fit of our method to the ground truth segmentation, except at the inferior borders of the SN. Judging from Table 1 and 2, this could be due to the individual variability of the histological data, or the fact that the MRI does not reveal equal amounts of tissue as shown in chemically stained histological data. Compared with the histological atlas, the limited accuracy of manual segmentation (intra- and inter-rater variability) can only make the MRI-based atlas a silver standard due to the limits of current MRI (i.e. resolution and partial volume effect). Although label fusion techniques, together with high field MRI (i.e. 7T) may mitigate these drawbacks, ultimately the extents of the nuclei are confirmed by intra-surgical electro-physiological recording. Due to the fact that the STN is much smaller than the other structures of the basal ganglia (i.e. GP or striatum), and the image resolution is on the scale of 1 mm^3, the kappa metric may not be perfectly appropriate to represent the full potential of this new technique. There are very few previous studies evaluating volumetric segmentation of the STN, RN, and SN with overlap metrics; most report 3D distance measures only. Upon consideration of the Euclidean distances between the automatic and manual segmentation and visual inspection, our segmentation quality is satisfactory. However, efforts could still be made to further improve the system in the future. First, although the FSE T2w image and T2*w images demonstrate similar contrast in the basal ganglia system, we would like to construct multi-modality templates that include both T1w and T2*w images for both healthy and PD brains in different age groups. This way, the variability in shape and in the nuclei contrasts due to aging or pathological changes can be better accounted for. Second, we believe that by adding geometric shape constraints and other image contrasts (i.e. quantitative susceptibility map), the segmentation accuracy could be enhanced. Last, we would like to compare the location of the segmented STN with electro-physiological recording to confirm its efficiency.

6 Conclusion

Upon visual inspection of the registered results using the original T1w-image-only framework, there was a coarse correspondence of the STN, SN, and RN between the warped atlas and the manual segmentations, but the geometric description is not sufficiently accurate according to the quantitative evaluation.

After incorporating MRI techniques that are capable of directly visualizing the STN and its adjacent SN and RN, we observed large improvements in separate stages of the atlas-based segmentation pipeline, as well as the segmentation performance of the entire system. This proved our original assumption that inter-subject (atlas-to-template or template-to-subject) registration with only T1w images is not sufficient for structures that are almost invisible on the T1w images, as far as the registration framework in [3] is concerned. In conclusion, we established a technique that automatically segments the STN, SN, and RN for STN deep brain stimulation, by combining MRI techniques that can directly delineate these nuclei, and a high resolution basal ganglia atlas that was defined from histological data. This framework was validated on 6 subjects (3 healthy and 3 PD patients), and is an improvement compared with the technique in [3].

References

[1] Brunenberg, E.J., Platel, B., Hofman, P.A., Ter Haar Romeny, B.M., Visser-Vandewalle, V.: Magnetic resonance imaging techniques for visualization of the subthalamic nucleus. J. Neurosurg. 115(5), 971–984 (2011)

[2] O'Gorman, R.L., Shmueli, K., Ashkan, K., Samuel, M., Lythgoe, D.J., Shahidiani, A., Jarosz, J.: Optimal MRI methods for direct stereotactic targeting of the subthalamic nucleus and globus pallidus. Eur. Radiol. 21(1), 130–136 (2011)

[3] Chakravarty, M.M., Sadikot, A.F., Germann, J., Bertrand, G., Collins, D.L.: Towards a validation of atlas warping techniques. Med. Image Anal. 12(6), 713–726 (2008)

[4] Chakravarty, M.M., Bertrand, G., Hodge, C.P., Sadikot, A.F., Collins, D.L.: The creation of a brain atlas for image guided neurosurgery using serial histological data. Neuroimage 30(2), 359–376 (2006)

[5] Holmes, C.J., Hoge, R., Collins, L., Woods, R., Toga, A.W., Evans, A.C.: Enhancement of MR images using registration for signal averaging. J. Comput. Assist. Tomogr. 22(2), 324–333 (1998)

[6] Collins, D.L., Evans, A.C.: Animal: Validation and applications of nonlinear registration-based segmentation. Int. J. Pattern Recogn. 11(8), 1271–1294 (1997)

[7] Studholme, C., Hill, D.L.G., Hawkes, D.J.: An overlap invariant entropy measure of 3D medical image alignment. Pattern Recogn. 32(1), 71–86 (1999)

[8] Sled, J.G., Zijdenbos, A.P., Evans, A.C.: A nonparametric method for automatic correction of intensity nonuniformity in MRI data. IEEE Trans. Med. Imaging 17(1), 87–97 (1998)

[9] Nyul, L.G., Udupa, J.K., Zhang, X.: New variants of a method of MRI scale standardization. IEEE Trans. Med. Imaging 19(2), 143–150 (2000)

[10] Coupé, P., Yger, P., Barillot, C.: Fast Non Local Means Denoising for 3D MR Images. In: Larsen, R., Nielsen, M., Sporring, J. (eds.) MICCAI 2006. LNCS, vol. 4191, pp. 33–40. Springer, Heidelberg (2006)

[11] Xiao, Y., Beriault, S., Pike, B.G., Collins, D.L.: Multi-contrast multi-echo FLASH MRI for targeting the subthalamic nucleus. Magn. Reson. Imaging (to appear)